Supplementary Material
Localization of fixed dipoles at high precision by accounting for sample drift during illumination

Fabian Hinterer,[1, a)] Magdalena C Schneider,[2, 3, a)] Simon Hubmer,[4] Montserrat López-Martínez,[2] Ronny Ramlau,[1] and Gerhard J Schütz[2]

[1)] *Johannes Kepler University, Institute of Industrial Mathematics, Linz, Austria*

[2)] *TU Wien, Institute of Applied Physics, Vienna, Austria*

[3)] *Janelia Research Campus, Howard Hughes Medical Institute, Ashburn, VA, USA*

[4)] *Johann Radon Institute Linz, Linz, Austria*

A. Mathematical Model

We use the same image formation model as in our previous publication[1], which in turn is based on[2]. A dipole point source can be characterized by its orientation (θ, ϕ) and its position (x, y, z), where θ denotes the inclination angle with respect to the optical axis, and ϕ denotes the azimuthal angle within the sample plane w.r.t to an arbitrary but fixed coordinate system. For our model, we consider a fluorophore positioned in the focal plane $(z = 0)$ with a fixed dipole orientation. In addition, we consider a possible unknown defocus d of the objective.

The dipole emission pattern can be expressed as an angular spectrum of plane waves. These plane waves, while propagating through the optical system, are refracted and reflected according to Snell's law and Fresnel equations. The infinity-corrected objective captures the emission light emanating radially from the source and directs it parallel to the optical axis through the back focal plane of the objective. We consider the electric field in the back focal plane (BFP) in Cartesian coordinates:

$$E_{\mathrm{BFP}}(\vec{x}_b) = E_{\mathrm{BFP}}(x_b, y_b) = E_{\mathrm{BFP}}(x_b, y_b; \theta, \phi). \tag{S1}$$

In this model, the BFP field only depends on the orientation of the emitter, as the lateral position will be modeled via tip-/tilt aberrations. Any wavefront deformation, either caused by aberration or deliberate distortion, is modeled by introducing additional phase factors[3]. We therefore define the aberration term $W_\xi(x, y)$ modeling tip/tilt aberrations and defocus (and possibly additional aberrations). The parameter vector $\xi = (x, y, d)$ collects the position of the emitter and the defocus, the parameters which we are later interested in estimating.

The light beam then enters the tube lens as an infinite parallel beam. The field at the focal plane of the tube lens is given by the Fourier transform of E_{BFP} multiplied with the phase factor introduced above,

$$E_\xi(\vec{x}_f) = \tfrac{1}{i\lambda f} e^{\frac{ik}{\lambda f}\|\vec{x}_f\|^2} \int E_{\mathrm{BFP}}(\vec{x}_b) e^{\frac{2\pi i}{\lambda} W_\xi(\vec{x}_b)} e^{-\frac{2\pi i}{\lambda f}\vec{x}_b \cdot \vec{x}_f} d\vec{x}_b\,, \tag{S2}$$

where f denotes the focal length of the tube lens and the subscript f indicates coordinates in the focal plane. The intensity distribution in the focal plane of the tube lens is given by the absolute value of the electric field,

$$I_\xi(\vec{x}_f) = |E_\xi(\vec{x}_f)|^2. \tag{S3}$$

We now consider the scenario where the emitter undergoes a lateral motion during the recording process. To model this motion, we define the path

$$\gamma : [0, T] \to \Omega \subset \mathbb{R}^2. \tag{S4}$$

The intensity measured at the detector plane is then the integrated intensity

$$\mathcal{I}_{\xi,\gamma}(\vec{x}_f) := \int_0^T |E_{\xi,\gamma(t)}(\vec{x}_f)|^2 dt, \tag{S5}$$

where

$$E_{\xi,\gamma(t)}(\vec{x}_f) := \tfrac{1}{i\lambda f} e^{\frac{ik}{\lambda f}\|\vec{x}_f\|^2} \int E_{\mathrm{BFP}}(\vec{x}_b) e^{\frac{2\pi i}{\lambda} W_{\xi,\gamma(t)}(\vec{x}_b)} e^{-\frac{2\pi i}{\lambda f}\vec{x}_f \cdot \vec{x}_b} d\vec{x}_b. \tag{S6}$$

Here, the motion $\gamma(t)$ at time t is incorporated into the aberration term $W_{\xi,\gamma(t)}$ as additional tip and tilt terms,

$$W_{\xi,\gamma(t)}(\vec{x}_b) = W_\xi(\vec{x}_b) + \gamma_1(t) Z_2(\vec{x}_b) + \gamma_2(t) Z_3(\vec{x}_b), \tag{S7}$$

where Z_2 and Z_3 denote the second and third Zernike polynomial in Noll's indices[4]. The remaining aberration term W_ξ is further expanded into Zernike polynomials Z_2, Z_3 and Z_4, modelling the position of the fluorophore and the defocus, both specified by the parameter ξ.

If 3D fiducial tracking is available, this information can easily be incorporated into the method. In this case, we model the path γ as

$$\gamma : [0, T] \to \Omega \subset \mathbb{R}^3 \tag{S8}$$

and the wavefront in (S7) is extended by an additional Zernike term Z_4 modelling defocus,

$$W_{\xi,\gamma(t)}(\vec{x}_b) = W_\xi(\vec{x}_b) + \gamma_1(t) Z_2(\vec{x}_b) + \gamma_2(t) Z_3(\vec{x}_b) + \gamma_3(t) Z_4(\vec{x}_b). \tag{S9}$$

For simulation and fitting purposes, we consider equation (S5) using a discrete representation of γ. We assume that we sample the motion at N uniformly spaced time steps,

[a)] corresponding authors: fabian.hinterer@indmath.uni-linz.ac.at, schneiderm2@hhmi.org

resulting in a measurement $\hat{\gamma} \in \Omega^N$. We can approximate the integral in (S5) by the sum

$$\mathcal{I}_{\xi,\hat{\gamma}}(\vec{x}_f) \equiv \sum_{k=1}^{N} \left| \int E_{\mathrm{BFP}}(\vec{x}_b) e^{\frac{2\pi i}{\lambda} W_{\xi,\hat{\gamma}_k}(\vec{x}_b)} e^{-\frac{2\pi i}{\lambda f} \vec{x}_f \cdot \vec{x}_b} d\vec{x}_b \right|^2, \tag{S10}$$

which is the superposition of the signal of N emitters and corresponds to (S5) being approximated with a midpoint rule at the supporting points $(\hat{\gamma}_k)_{k=1}^N$. The desired amplitude of (S10) will be introduced with an appropriate scaling factor.

B. Simulations

Unless otherwise specified, we use the same set of parameters and assumptions as previously described in[1], the key aspect of which is an astigmatic and low-aperture (NA=0.7) imaging model.

We model an air objective ($n_2 = 1$) with a magnification of 60x and a focal length of 3 mm, and a tube lens with a focal length of $f = 180$ nm. We assume a biological sample with a refractive index of water ($n_2 = 1.33$), and dyes with an emission wavelength of $\lambda = 680$ nm.

As input parameters for our simulated data we randomly sample values for the emitter's position (x^*, y^*) and defocus d^* from uniform distributions. Further, we assume that dipole orientation (θ^*, ϕ^*) is uniformly distributed on the unit sphere. We use the superscript * to denote a ground truth variable. Position is sampled within ± 1 pixel from the center (corresponding to the optical axis). The defocus is chosen randomly between ± 500 nm.

We consider three different types of sample drift: Diffusion, linear drift in direction of $\pi/4$ w.r.t. to the x-axis and oscillation in x-direction. For the oscillation, we use a frequency of 10 oscillations per frame.

We model the astigmatic distortion by adding an additional Zernike polynomial Z_6 to the phase factor (S7) and setting the corresponding Zernike coefficient to 0.11λ.

For the simulation of the data, we calculate the intensity distribution (S10) within an analysis region of 17×17 pixels using $N = 500$ discretization points in time. To reduce numerical inaccuracies, we calculate the intensity distribution on a subpixel grid and then sum up over the individual pixel bins. We use a pixel size of 108 nm and an oversampling factor of 9 for the subpixel grid. We scale the total intensity (i.e. the sum of all pixel values) to the desired photon count and then apply Poissonian shot noise. As photon count we select 10^5 photons in all simulations. All simulations were carried out in MATLAB.

C. Parameter estimation

Given a possibly noisy input image $\mathcal{I}$, we want to retrieve an estimate of the parameter vector ξ^*, containing the position of the emitter and the defocusing of the optical system.

First, we subtract the mean background signal b^2 from the image, which we estimate from the mean signal of an image containing no fluorophore signal. The total number of detected photons from a fluorophore is estimated by summing over all pixels of the noise-corrected image. For the following fitting procedure, we normalize the photon count in the images. As additional input, we require an estimate $\hat{\gamma}$ of the motion and an estimate $(\hat{\theta}, \hat{\phi})$ of the dipole orientation of the emitter. We assume that the errors for both the inclination and azimuthal angle are distributed normally with mean 0 and variance 2°. The estimate $\hat{\gamma}$ of the motion is possibly contaminated with noise, which is assumed to follow a Gaussian distribution. We proceed by minimizing the negative log-likelihood using the Matlab function *fminunc*. The log-likelihood function is given by

$$\ell(\xi) = \sum \left(\mathcal{I} \cdot \ln(\mathcal{I}_{\xi,\hat{\gamma}}) - \mathcal{I}_{\xi,\hat{\gamma}} - \ln(\mathcal{I}!) \right) \tag{S11}$$

where $\mathcal{I}_{\xi,\hat{\gamma}}$ is the pixelated intensity distribution (S10) with the parameters ξ. Note that all expressions in (S11) are matrix-valued and the operations, including multiplication, should be understood component-wise. The sum is then performed over all matrix elements. We refer to Eq. (27) in[5] for a derivation of the likelihood function. By applying the logarithm, we then arrive at the log-likelihood function. For the fit, the normalized image $\mathcal{I}_\xi$ of the PSF is calculated using an oversampling factor of 3. As initial guess for the optimization procedure we select randomly chosen values from the admissible set of parameters. Minimizing the negative log-likelihood yields an estimate

$$\hat{\xi} = (\hat{x}, \hat{y}, \hat{d}) = \operatorname{argmin}(-\ell(\xi)) \,. \tag{S12}$$

We repeat the simulation and fitting procedure n times for each data point. The quantities we are interested in are the localization accuracy, which is defined by the mean error $\mu_x = \frac{1}{n} \sum (\hat{x} - x^*)$ and the localization precision σ_x, which is defined as the standard deviation of the estimates from the mean, $\sigma_x^2 := \frac{1}{n} \sum (\hat{x} - x^* - \mu_x)^2$. The quantities for the y-position and defocus are defined analogously. Note that the localization precision and accuracy are typically defined for an isolated emitter that is imaged n times with only the realization of the shot noise differing in each frame[6]. In contrast, we calculate the precision and accuracy for n emitters, where the underlying parameters are randomly sampled. Since we are mainly interested in an overall precision, we believe this quantity to be more relevant for our purposes.

[1] F. Hinterer, M. C. Schneider, S. Hubmer, M. López-Martinez, P. Zelger, A. Jesacher, R. Ramlau, and G. J. Schütz, "Robust and bias-free localization of individual fixed dipole emitters achieving the cramér rao bound for applications in cryo-single molecule localization microscopy," PloS one **17**, e0263500 (2022).

[2] D. Axelrod, "Fluorescence excitation and imaging of single molecules near coated surfaces: A theoretical study," Journal of microscopy **247**, 147–60 (2012).

[3] J. Goodman, *Introduction to Fourier Optics*, Electrical Engineering Series (McGraw-Hill, 1996).
[4] R. J. Noll, "Zernike polynomials and atmospheric turbulence∗," J. Opt. Soc. Am. **66**, 207–211 (1976).
[5] R. Ober, S. Ram, and E. Ward, "Localization accuracy in single-molecule microscopy," Biophysical journal **86**, 1185–200 (2004).
[6] H. Deschout, F. Cella Zanacchi, M. Mlodzianoski, A. Diaspro, J. Bewersdorf, S. T. Hess, and K. Braeckmans, "Precisely and accurately localizing single emitters in fluorescence microscopy," Nature methods **11**, 253—266 (2014).

SUPPLEMENTARY FIGURES

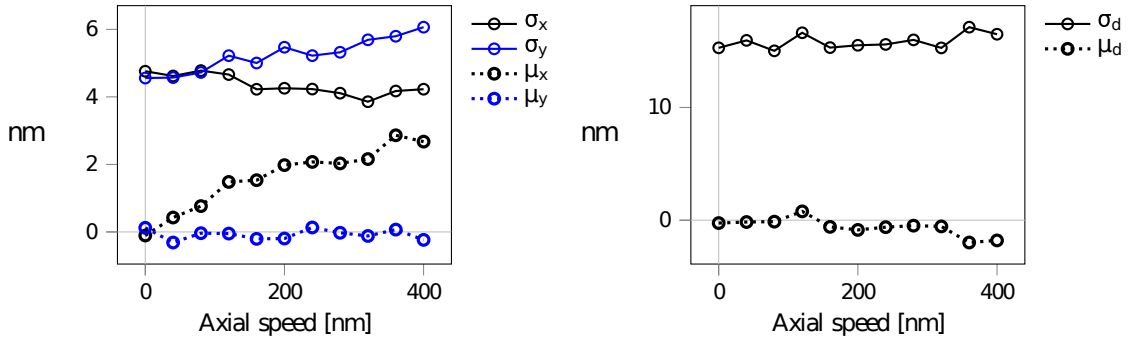

FIG. S1. **Presence of axial drift**. In addition to lateral drift (linear in x-direction with a speed of 200 nm per frame), we assume linear axial drift with a speed ranging from $0 - 400$ nm per frame. For the fitting procedure, we only assume knowledge about the lateral drift trajectory. In the left panel, we plot localization errors for the lateral components, and in the right panel for the defocus. Note that the astigmatic distortion causes opposing trends for the localization precision measured in x- and y-directions, hence both components are plotted. Each data point represents 1000 simulations.

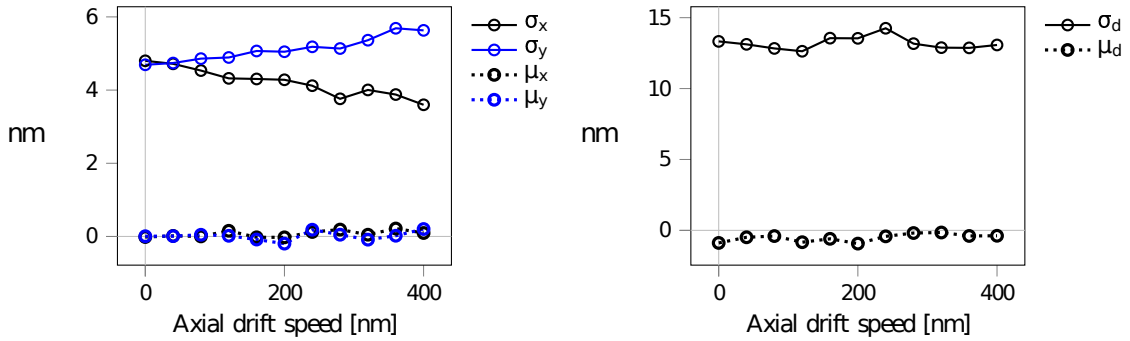

FIG. S2. **3D fiducial tracking**. In addition to lateral drift (linear in x-direction with a speed of 200 nm per frame), we assume linear axial drift with a speed of up to 400 nm per frame. We assume that 3D fiducial tracking is available. In the left panel, we plot localization errors for the lateral components, and in the right panel for the defocus. Each data point represents 1000 simulations.